Progress In Electromagnetics Research B, Vol. 47, 383–404, 2013

ANALYSIS OF SCATTERING FROM THREE-DIMENSIONAL OBJECTS BURIED BELOW A RANDOM ROUGH SURFACE BY MONTE-CARLO MPSTD METHOD

Wei Liu, Yueyang Dai, and Xiaobang Xu*

Holcombe Department of Electrical and Computer Engineering, Clemson University, Clemson, SC 29634-0915, USA

Abstract—This paper presents a Monte-Carlo multidomain pseudospectral time-domain (MPSTD) algorithm developed for the analysis of scattering from a three dimensional (3D) object buried below a random rough surface separating two half spaces. In the development, special attention is paid to the 3D computation domain decomposition and subdomain mapping involving the random rough surface as well as the subdomain patching along the rough surface. The Mote-Carlo MPSTD algorithm is then employed to determine the scattering of 3D objects of various shapes and electromagnetic properties; embedded in the lower half space with different permittivity and the roughness of the random rough surface may vary. Sample numerical results are presented, validated, and analyzed. Through the analysis, it is observed that the roughness of the random rough surface and the electromagnetic properties of the lower half space can significantly affect the scattered signature of the buried object.

1. INTRODUCTION

Analysis of electromagnetic scattering of buried objects has been widely used in subsurface investigations. Since the earth surface is a random rough surface in reality, it is important to incorporate the roughness of the surface into the analysis. In the past, analytic methods including the Kirchhoff approximation (KA) [1], the small perturbation method (SPM) [2], and the small slope approximation (SSA) [3], have been employed for studying the scattering from a random rough surface alone in absence of buried objects, based on

Received 1 October 2012, Accepted 9 January 2013, Scheduled 12 January 2013

* Corresponding author: Xiaobang Xu (ecexu@clemson.edu).

certain approximations. For analyzing the scattering of objects near a random rough surface, analytic methods, numerical and hybrid techniques have been developed. SPM was employed to study scattering by a cylinder buried beneath a slightly rough surface in frequency domain [4, 5]. As pointed out in [4], "Analytical solutions, unlike numerical techniques, are unfortunately limited to canonical geometries or small perturbations from a canonical geometry. Nevertheless, analytical solutions are valuable in that they do not require a discretization of the geometry and can provide a benchmark for comparison with numerical solutions." Surface integral equations were formulated and solved by the method of moments (MoM) for the two-dimensional (2D) [6], and three-dimensional (3D) [7, 8] scattering problems. As a method to improve the calculation efficiency, steepest descent fast multipole method (SDFMM) has been implemented together with MoM to study the electromagnetic scattering by 3D objects near a rough surface [9, 10]. Also, various hybrid techniques have been formulated for studying the 3D scattering problems, including a hybrid MoM and sparse matrix canonical grid (SMCG) method [11], a hybrid MoM and modified PO algorithm [12], and a hybrid Kirchhoff approximation and MoM [13–15]. All of these numerical and hybrid techniques are developed and employed for solving the scattering problems in frequency domain.

As an effective time-domain algorithm, the Monte-Carlo finite difference time-domain method (FDTD) method has been developed for determining the scattering from a moderately rough surface alone [16] and the bistatic scattering from a 3D object over a random rough surface [17, 18]. In contrast to the surface integral equation formulation, the FDTD approach is more effective for modeling complex inhomogeneous geometries. In addition, either pulsed or continuous wave illumination can be used in the FDTD approach and propagation of the fields can be observed in the time domain. However, this approach has its drawbacks. As indicated in [19, 20], the FDTD method based on the classical Yee scheme introduces the "staircase nature"; and this method requires a grid density of 10 to 20 cells per minimum wavelength to ensure its accuracy [21].

In recent years, the pseudospectral time-domain (PSTD) method [22] has been developed and successfully applied to solve various problems of practical interest. It has been used for the analysis of scattering of 2D and 3D objects in an open space [23–28]. In addition, the scattering of objects buried below a *planar* surface has been studied by a Fourier PSTD approach [21, 29, 30], and a multidomain PSTD (MPSTD) algorithm has been developed for the analysis of scattering of 2D objects buried below a planar

or undulating surface [31]. As illustrated by a number of numerical experiment results reported in the literature [21, 26], the PSTD algorithm requires significantly less CPU time and core memory for the same or even higher accuracy, being compared with the FDTD method. Furthermore, in the MPSTD formulation, the computation domain is divided into non-overlapping subdomains conformal to the problem geometry [26, 31], which enables one to treat complex geometry with great flexibility. This nature warrants a high potential of application of the MPSTD method in the analysis of scattering involving random rough surfaces, the geometry of which is apparently complex and needs special attention. But to the best knowledge of the authors, the MPSTD method that is more effective than the classic FDTD approach had not been applied in combination with the Monte-Carlo method for determining the scattering of objects buried below a *random* rough surface, which may better simulate media interfaces in reality and is of practical interest, until most recent time.

Most recently, a Monte-Carlo MPSTD algorithm has been developed for investigating the scattering of a cylinder buried below a random rough surface [32]. But the investigation was limited to a 2D configuration.

However, in reality, most of the buried objects are three dimensional. Therefore, in this paper, the 2D Monte-Carlo MPSTD algorithm presented in the authors' previous work [32] is further developed for studying the scattering of 3D objects buried below a *random rough surface*. The rest of this paper is organized as the follows. In Section 2, we formulate the 3D Monte-Carlo MPSTD algorithm, in which special attention is paid to the treatment of the random rough surface. Then, employing the 3D Monte-Carlo MPSTD numerical technique developed, numerical results are obtained, presented, and analyzed in Section 3. Finally, conclusions are drawn in Section 4.

2. FORMULATION OF THE 3D MONTE-CARLO MPSTD TECHNIQUE

Figure 1 shows a dielectric sphere, as an example of a 3D object of arbitrary shape, buried below a random rough surface that separates two homogeneous spaces. The upper half-space is characterized by $(\mu_0,\ \varepsilon_{r1}\varepsilon_0)$ and the lower half-space is characterized by $(\mu_0,\ \varepsilon_{r2}\varepsilon_0)$. The buried object is illuminated by a plane wave incidence. Under these conditions, the electromagnetic fields must satisfy the Maxwell's equation,

$$\nabla \times \vec{E} = -\mu \frac{\partial \vec{H}}{\partial t}, \tag{1}$$

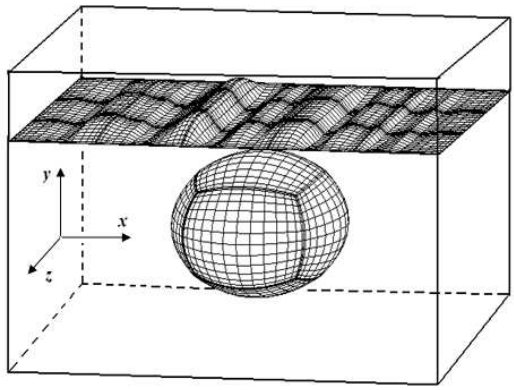

Figure 1. A 3D object buried below a random rough surface.

$$\nabla \times \vec{H} = \varepsilon \frac{\partial \vec{E}}{\partial t} + \sigma \vec{E} + \vec{J}. \tag{2}$$

The scattering from the 3D object buried below a random rough surface is to be determined by a Monte-Carlo MPSTD algorithm formulated in this section.

2.1. Formulation of the 3D MPSTD Algorithm

In this section, first, the major steps of the general 3D MPSTD algorithm are briefly outlined. Then, we focus on the treatment of a random rough surface involved in the analysis of scattering of a 3D object buried below it. In particular, the 3D computation domain decomposition, the subdomain mapping, and the subdomain patching along the random rough surface are derived.

2.1.1. Outline of the General 3D MPSTD Algorithm

The first step of the MPSTD algorithm is to divide the computation domain into non-overlapping subdomains, conforming to the problem geometry including a random rough surface involved in this analysis. In order to truncate the unbounded medium and confine the solution in a finite computation domain, an absorbing boundary condition (ABC) is introduced by implementing a well-posed perfectly matched layer (PML) [33–35] surrounding the "regular" region. Then, each subdomain in the (x, y, z) coordinates is mapped into a unit cube in the (ξ, η, ζ) coordinates by means of coordinate transformation. In the transformed (ξ, η, ζ) coordinates, the Chebyshev-Gauss-Lagrange

(CGL) points are chosen as the grid points. Making use of the coordinate transformation $\xi = \xi(x, y, z)$, $\eta = \eta(x, y, z)$, and $\zeta = \zeta(x, y, z)$, the Maxwell's Equations (1) and (2) in the (x, y, z) coordinates can be rewritten in the (ξ, η, ζ) coordinate system. And the electromagnetic field quantities and their spatial derivatives in the (ξ, η, ζ) coordinates are represented by a tensor-product Chebyshev-Lagarange polynomial [22]. To take care of the time derivatives of the fields appearing in Equations (1) and (2), a Runge-Kutta method [22, 31] is employed to update the solutions in time domain.

2.1.2. Treatment of the Random Rough Surface

In the formulation of the Monte-Carlo MPSTD algorithm for studying the scattering of a 3D object buried below a random rough surface, special attention is paid to the treatment of the random rough surface as described below.

2.1.2-1 Generation of Random Rough Surface Profile and Its Matching with CGL Points

Different from the previously published MPSTD analysis, which mainly analyzed the scattering of buried objects under flat or undulated surfaces, this work and the authors' previous one [32] involve a random rough surface. As the first trial to introduce a random rough surface into the Monte-Carlo MPSTD algorithm, the random rough surface is generated in x direction with Gaussian spectrum profile [36, 37],

$$y = f(x_m) = \frac{1}{L} \sum_{n=-N/2+1}^{N/2} b_n \exp\left(i\frac{2\pi nm}{N}\right), \tag{3}$$

where $x_m = mL/N$, $(m = 1, 2, \ldots, N)$ in which L is the length of the rough surface, and b_n is the inverse Fourier transform coefficient defined in terms of the correlation length l_c and the *rms* height of the random rough surface. A sample random rough surface generated is illustrated in Figure 1.

As pointed out in [32], the profile $y = f(x_m)$ is generated as a function of evenly distributed x_m. But in a MPSTD subdomain that is partially bounded by the rough surface, the profile y_{mapped} is a function of x_{mapped}, which are related to the CGL points in the (ξ, η, ζ) coordinates by the coordinate transformation. Since x_m are uniformly distributed but x_{mapped} are not, they are normally different; hence the two profiles of $y = f(x_m)$ and y_{mapped} in general do not coincide. To match these two profiles, an interpolation technique is used as described in [32].

2.1.2-2. Three-dimensional Subdomain Division and Subdomain Mapping

When a random rough surface and a 3D object with curved surface are involved in the analysis, the subdomain division, mapping of a subdomain from the (x, y, z) coordinates to the (ξ, η, ζ) coordinates, and choosing of the anchor points for the mapping are particularly important. Corresponding to certain shape of the object and the rough surface profile, an appropriate division of the computation domain and proper selection of the anchor points can help reduce the number of subdomains and thereby improve the computational efficiency. For a general curved hexahedral subdomain, a curvilinear coordinate transformation in terms of the Lagrange polynomials [22, 26] can be employed,

$$x = \sum_{p=0}^{P}\sum_{q=0}^{Q}\sum_{r=0}^{R} x_{pqr}\phi_p^{(P)}(\xi)\phi_q^{(Q)}(\eta)\phi_r^{(R)}(\zeta), \tag{4a}$$

$$y = \sum_{p=0}^{P}\sum_{q=0}^{Q}\sum_{r=0}^{R} y_{pqr}\phi_p^{(P)}(\xi)\phi_q^{(Q)}(\eta)\phi_r^{(R)}(\zeta), \tag{4b}$$

$$z = \sum_{p=0}^{P}\sum_{q=0}^{Q}\sum_{r=0}^{R} z_{pqr}\phi_p^{(P)}(\xi)\phi_q^{(Q)}(\eta)\phi_r^{(R)}(\zeta), \tag{4c}$$

where x_{pqr}, y_{pqr}, and z_{pqr} are the anchor points.

To illustrate the procedure of the subdomain division and selection of anchor points for subdomain mapping, we use a dielectric sphere below a random rough surface as an example, the geometry of which is depicted in Figure 1. As the first step of the 3D MPSTD formulation, the computation domain is divided into 216 non-overlapping hexahedral subdomains. Sample subdomains that contain the rough surface and the dielectric sphere are depicted in Figure 2(a). After the division, anchor points for each subdomain are chosen for the subdomain mapping. For the subdomains that are partially bounded by the random rough surface, to accurately model the complex geometry, sufficient anchor points are needed. In this work, 90 anchor points are chosen in each of these subdomains. Then, using these anchor points in Equations(4a)–(4c), a hexahedral subdomain in the (x, y, z) coordinate system is successfully mapped to a unit cube in the (ξ, η, ζ) coordinate system, as depicted in Figure 2(b).

2.1.2-3. Subdomain Patching in 3D Computation Domain

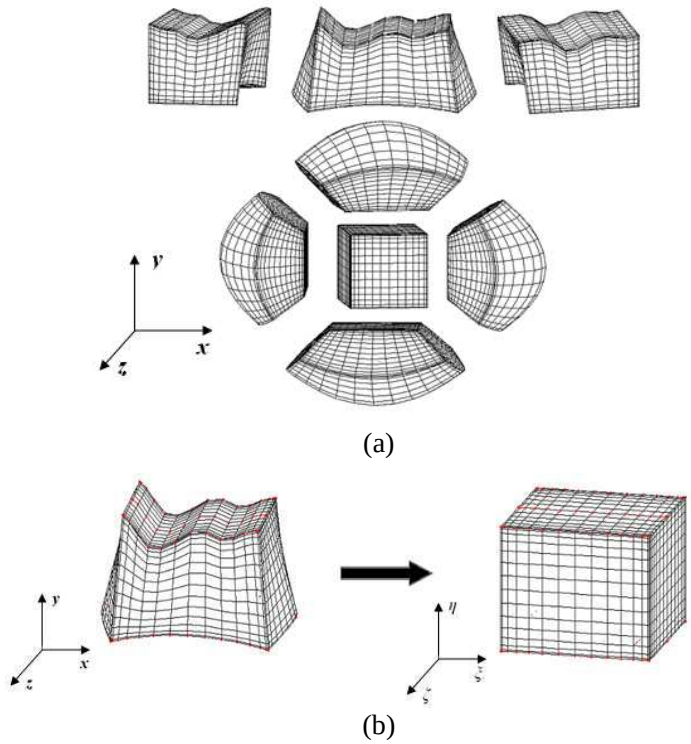

Figure 2. Computation domain division and subdomain mapping. (a) Sample subdomains. (b) Coordinate mapping.

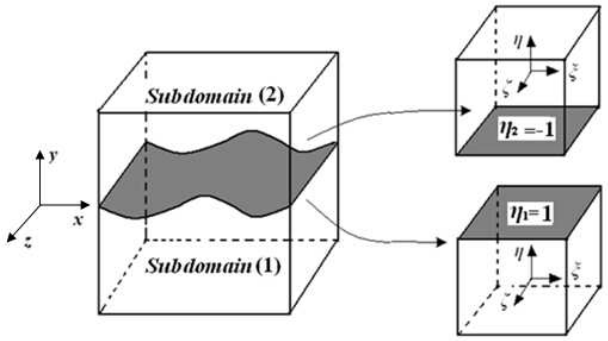

Figure 3. Subdomain mapping of two subdomains separated by a random rough surface.

Two subdomains, which are separated by a random rough surface, in the (x, y, z) coordinate system is illustrated in Figure 3. Following the procedure described above, each subdomain is mapped to a unit cube in the (ξ, η, ζ) coordinate system. The bottom surface of subdomain (2) and the top surface of (1) are mapped to the $\eta = -1$ and $\eta = 1$ surface of the unit cube, respectively. Note that the interface separating these two subdomains is a random rough surface, special attention should be paid to the subdomain patching there. To satisfy the boundary conditions, which require continuity of the tangential components of the electric and magnetic field at the interface, we need to identify the tangential and normal unit vectors at the interface first, and then use them to determine the tangential and normal components of the fields.

The unit vector normal to the η plane is given by

$$\hat{n} = \frac{1}{\sqrt{\eta_x^2 + \eta_y^2 + \eta_z^2}} \left(\eta_x \hat{x} + \eta_y \hat{y} + \eta_s \hat{z}\right), \tag{5}$$

and the three unit vectors tangential to the interface are

$$\begin{cases} \hat{t}_1 = \frac{1}{\sqrt{\eta_y^2+\eta_z^2}} \left(\eta_z \hat{y} - \eta_y \hat{z}\right), \\ \hat{t}_2 = \frac{1}{\sqrt{\eta_x^2+\eta_z^2}} \left(-\eta_z \hat{x} + \eta_x \hat{z}\right), \\ \hat{t}_3 = \frac{1}{\sqrt{\eta_x^2+\eta_y^2}} \left(\eta_y \hat{x} - \eta_x \hat{y}\right), \end{cases} \tag{6}$$

in which η_x, η_y, and η_z are the partial derivatives of η with respect to x, y and z. It is noted that the three unit vectors in (6) are not linearly independent. Therefore, after two out of the three tangential field components along $(\hat{t_1}, \hat{t_2}, \hat{t_3})$ are set to be continuous, the third one is automatically continuous.

Using the unit vectors given in (5) and (6), the tangential and normal components of the fields can be obtained by taking dot product of the corresponding unit vector with the fields. Then, by enforcing the continuity of the tangential components along the unit vectors $\hat{t_1}$ and $\hat{t_2}$; and leaving the normal components remain unchanged, we have

$$\tilde{H}_{t1}^{(1)}, \tilde{H}_{t1}^{(2)} = \frac{1}{2}\left(H_{t1}^{(1)} + H_{t1}^{(2)}\right), \quad \tilde{H}_{t2}^{(1)}, \tilde{H}_{t2}^{(2)} = \frac{1}{2}\left(H_{t2}^{(1)} + H_{t2}^{(2)}\right), \tag{7}$$

$$\tilde{E}_{t1}^{(1)}, \tilde{E}_{t1}^{(2)} = \frac{1}{2}\left(E_{t1}^{(1)} + E_{t1}^{(2)}\right), \quad \tilde{E}_{t2}^{(1)}, \tilde{E}_{t2}^{(2)} = \frac{1}{2}\left(E_{t2}^{(1)} + E_{t2}^{(2)}\right), \tag{8}$$

$$\tilde{E}_n^{(1)} = E_n^{(1)}, \quad \tilde{H}_n^{(1)} = H_n^{(1)}, \tag{9}$$

$$\tilde{E}_n^{(2)} = E_n^{(2)}, \quad \tilde{H}_n^{(2)} = H_n^{(2)}, \tag{10}$$

where the tilted variables are the tangential and normal components after the subdomain patching at each time step, the untitled variables

are the components before the patching, and the super script denote the subdomain where the field components are located.

Solving Equations (7)–(10), the updated field components in subdomains (1) and (2) are obtained. The updated field components in subdomain (1) along the rough surface are

$$\tilde{E}_x^{(1)} = \frac{1}{2}\left(E_x^{(1)} + E_x^{(2)}\right) + \frac{\eta_x^2\left(E_x^{(1)} - E_x^{(2)}\right) + \eta_x\eta_y\left(E_y^{(1)} - E_y^{(2)}\right) + \eta_x\eta_z\left(E_z^{(1)} - E_z^{(2)}\right)}{2\left(\eta_x^2 + \eta_y^2 + \eta_z^2\right)}, \quad (11)$$

$$\tilde{E}_y^{(1)} = \frac{1}{2}\left(E_y^{(1)} + E_y^{(2)}\right) + \frac{\eta_x\eta_y\left(E_x^{(1)} - E_x^{(2)}\right) + \eta_y^2\left(E_y^{(1)} - E_y^{(2)}\right) + \eta_y\eta_z\left(E_z^{(1)} - E_z^{(2)}\right)}{2\left(\eta_x^2 + \eta_y^2 + \eta_z^2\right)}, \quad (12)$$

$$\tilde{E}_z^{(1)} = \frac{1}{2}\left(E_z^{(1)} + E_z^{(2)}\right) + \frac{\eta_x\eta_z\left(E_x^{(1)} - E_x^{(2)}\right) + \eta_y\eta_z\left(E_y^{(1)} - E_y^{(2)}\right) + \eta_z^{(2)}\left(E_z^{(1)} - E_z^{(2)}\right)}{2(\eta_x^2 + \eta_y^2 + \eta_z^2)}, \quad (13)$$

$$\tilde{H}_x^{(1)} = \frac{1}{2}\left(H_x^{(1)} + H_x^{(2)}\right) + \frac{\eta_x^2\left(H_x^{(1)} - H_x^{(2)}\right) + \eta_x\eta_y\left(H_y^{(1)} - H_y^{(2)}\right) + \eta_x\eta_z\left(H_z^{(1)} - H_z^{(2)}\right)}{2\left(\eta_x^2 + \eta_y^2 + \eta_z^2\right)}, \quad (14)$$

$$\tilde{H}_y^{(1)} = \frac{1}{2}\left(H_y^{(1)} + H_y^{(2)}\right) + \frac{\eta_x\eta_y\left(H_x^{(1)} - H_x^{(2)}\right) + \eta_y^2\left(H_y^{(1)} - H_y^{(2)}\right) + \eta_y\eta_z\left(H_z^{(1)} - H_z^{(2)}\right)}{2\left(\eta_x^2 + \eta_y^2 + \eta_z^2\right)}, \quad (15)$$

$$\tilde{H}_z^{(1)} = \frac{1}{2}(H_z^{(1)} + H_z^{(2)}) + \frac{\eta_x\eta_z\left(H_x^{(1)} - H_x^{(2)}\right) + \eta_y\eta_z\left(H_y^{(1)} - H_y^{(2)}\right) + \eta_z^{(2)}\left(H_z^{(1)} - H_z^{(2)}\right)}{2(\eta_x^2 + \eta_y^2 + \eta_z^2)}. \quad (16)$$

The updated electric and magnetic field components in subdomain (2) can be expressed by equations in the same form as Equations (11)–(16) with the super scripts 1 and 2 exchanged. Similar procedures can be implemented to obtain the updating equations for interfaces along other directions. For the subdomain patching along

the interfaces normal to ξ and ζ direction, after going through a similar procedure, the updating equations can be obtained by replacing η by ξ and ζ respectively in Equations (11)–(16).

2.2. Monte-Carlo Statistic Average

Since a *random* rough surface is involved in this work, a statistic average of the scattering of the buried 3D object below the rough surface needs to be determined. The Monte-Carlo method (MCM), which is also known as the method of statistical trials [38], has been used in the past together with an integral equation formulation in the frequency domain [9] and with the FDTD method in the time domain [16, 17] for the analysis of electromagnetic scattering involving a random rough surface. Most recently, a Monte-Carlo MPSTD algorithm is developed for the analysis of scattering from a 2D cylinder buried below a random rough surface [32]. In this work, the Monte-Carlo MPSTD algorithm is extended for studying the scattering of a 3D object buried below a random rough surface. It is carried out by the following steps. First, a set of random rough surfaces with Gaussian spectrum is generated. Then, the MPSTD algorithm formulated above is employed to determine the scattering of the buried object below each of the rough surfaces generated. And finally, the statistic average of the scattering is determined. To make sure that the Monte-Carlo statistic average results converge, numerical tests are performed and the results are presented in the next section.

3. NUMERICAL RESULTS AND DISCUSSIONS

In this section, we present numerical results of scattering of a 3D object buried below a random rough surface separating two half spaces. The upper half space is taken to be free space, and the lower one is a dielectric medium with various relative permittivity ε_{r2}. The excitation is a TM_z plane wave normal incidence, the time function of which is the first derivative of the Blackman-Harris window (BHW) function [21],

$$f(t) = \begin{cases} -\sum_{n=1}^{3} \frac{n\pi}{T} a_n \sin\left(\frac{2n\pi t}{T}\right), & 0 < t < T, \\ 0, & \text{else}, \end{cases} \tag{17}$$

where $a_1 = -0.488$, $a_2 = 0.145$, $a_3 = -0.01022222$, and $\frac{1}{T} = \frac{f_c}{1.55}$. In all the numerical examples presented in this section, the central frequency $f_c = 100\,\text{MHz}$, unless otherwise specified.

3.1. Validation of the MPSTD Algorithm

To validate the MPSTD algorithm developed, we introduce a *virtual* random rough surface placed along $y = 0$ and the half spaces above and below it are both set to be free space. In the first example, we consider the scattering of a dielectric cube, which is of side length 0.6 m, centered at (0, −0.9, 0), and characterized by $\mu_r = 1$, $\varepsilon_r = 4$ and $\sigma = 0$. It is illuminated by a TM_z plane wave propagating in $-y$ direction, the time function of which is the first derivative of BHW function with central frequency 200 MHz. At two observation points, one is below and the other is above the virtual rough surface, such calculated MPSTD results of the total field E_z are compared with the free-space results as well as those obtained using the FDTD method. From the comparison illustrated in Figures 4(a) and (b), one sees an excellent agreement between the three sets of data, as expected.

In the second example, we consider a lossy dielectric sphere, which is of radius 2 m, centered at (0, −3, 0), and characterized by $\mu_r = 1$, $\varepsilon_r = 4$ and $\sigma = 0.002$. The incident wave is with $f_c = 50$ MHz. At two observation points, one is below and the other is above the virtual rough surface, the MPSTD results of the total field E_z are compared with the free-space results as well those obtained using the FDTD method. The comparison is illustrated in Figures 5(a) and (b), where an excellent agreement between the three sets of data is observed.

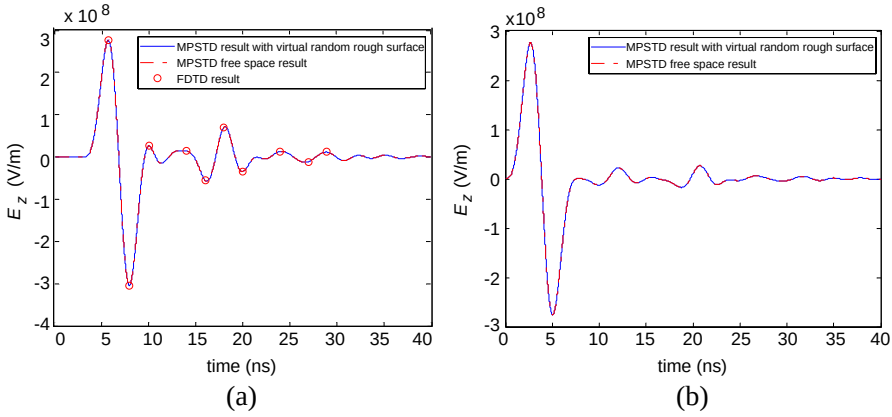

Figure 4. Scattering of a dielectric cube below a virtual random rough surface compared with the free-space results as well as the FDTD results. (a) At (0, −0.3, 0). (b) At (0, 0.6, 0).

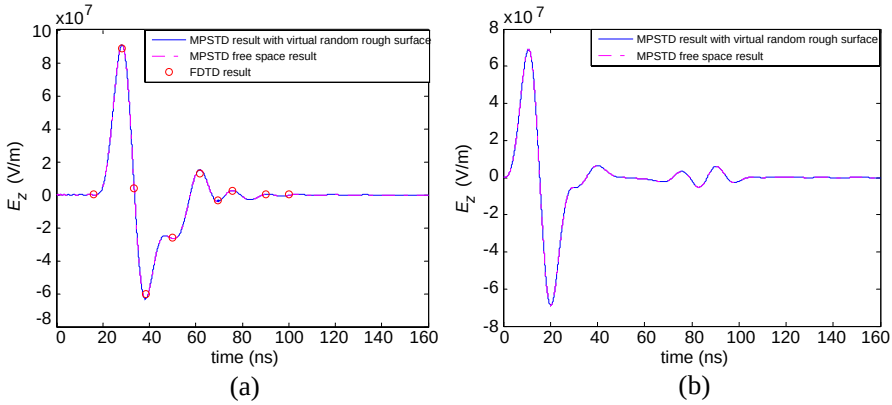

Figure 5. Scattering of a dielectric sphere below a virtual random rough surface compared with the free-space results as well as the FDTD results. (a) At (0, −3, −2.5). (b) At (0, 2, 0).

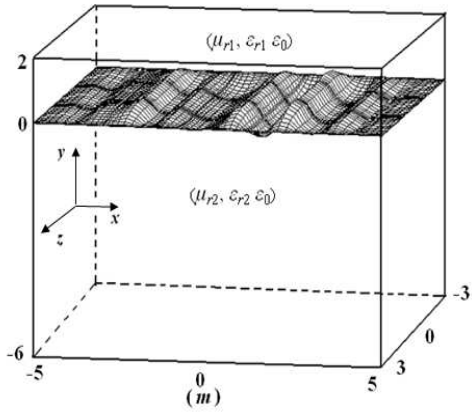

Figure 6. 3D computation domain containing a random rough surface.

3.2. Convergence Test for Scattering from a Random Rough Surface

To make sure that the numerical results of the 3D Monte-Carlo MPSTD technique converges, first, we employ it for the analysis of scattering of a random rough surface, which is of correlation length $l_c = 0.45\,\text{m}$, the *rms* height $h_{rms} = 0.2\,\text{m}$ and located within $-4 \leq x \leq 4$, $-3 \leq z \leq 3$. The upper half space is free space, and the

lower half space is a medium with relative permittivity $\varepsilon_{r2} = 3$. The computation domain (PML regions is not included for simplicity) is shown in Figure 6.

A set of N random rough surfaces is generated, the MPSTD numerical technique is employed N times for determining the scattering of each of the random rough surfaces, and then the Monte-Carlo statistic average is obtained. Such obtained electric field E_z observed at (0, 2, 0) and (−3, 2, 0) are presented in Figures 7(a) and (b). From the data presented in the figures, one notes that the numerical results have a significant change when N is increased from 1 to 10, but the change becomes very little when N is further increased from 10 to 13, which verifies the convergence of the Monte-Carlo MPSTD numerical technique after it is executed 10 times.

3.3. Scattering of a PEC Cube Buried below a Random Rough Surface

Next, we present the numerical results of scattering of a PEC cube with side length of 2 m and centered at (0, −3, 0), buried below a random rough surface, which is of the same parameters as that used in the previous sub-section. The computation domain is illustrated in Figure 8(a). In Figure 8(b), we present the numerical results of E_z observed at (−5, 2, 2) for the lower half space relative permittivity ε_{r2} varying from 3 to 1. From the data presented in the figure, one observes that as ε_{r2} decreases from 3 to 2, then to 1.5, and finally to 1, the results gradually reduce to that for the cube located in free space, as expected.

One notes that the incident wave propagates to impinge the

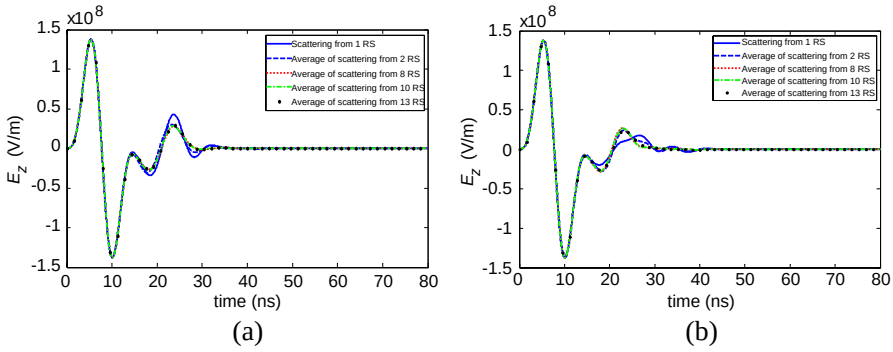

Figure 7. Convergence test for the scattering of a random rough surface. (a) At (0, 2, 0). (b) At (−3, 2, 0).

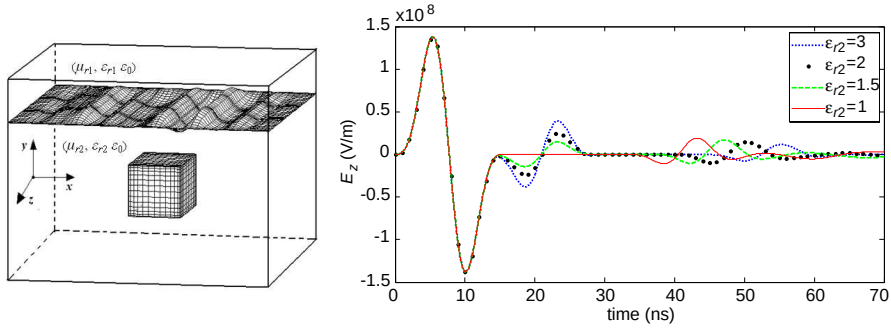

Figure 8. Scattering from a PEC cube buried below a random rough surface. (a) Geometry of the 3D computation domain. (b) E_z observed at $(-5, 2, 2)$ for various ε_{r2}.

random rough surface first and then the buried object; after that, the wave is scattered back to reach the observation point at $y = 2$ from the rough surface along $y = 0$ and then from the buried cube, the upper surface of which is along $y = -2$. Due to such a time sequence, the field depicted in this figure represents the incident wave for $t < 13\,\text{ns}$, the scattered wave by the rough surface for $13\,\text{ns} < t < 26\,\text{ns}$, and then the wave scattered by the buried cube for $t > 26\,\text{ns}$. Therefore, for $t < 13\,\text{ns}$, the curves corresponding to the four different values of ε_{r2} are identical because they are all the incident wave that is not affected by ε_{r2}; then for $13\,\text{ns} < t < 26\,\text{ns}$, the magnitudes of the fields are different due to the effect of the different lower half space relative permittivity ε_{r2} on the scattering from the rough surface; and finally, for $t > 26\,\text{ns}$, as ε_{r2} increases, there is a time delay of the wave propagating in the lower half space. This is due to the fact that the electromagnetic wave propagates at a slower speed in a medium with higher relative permittivity.

To illustrate the plane wave propagation through the random rough surface and its scattering by the PEC cube, spatial distribution of the electric field E_z on the $z = 0$ plane at two specific moments $t = 15\,\text{ns}$ and $t = 30\,\text{ns}$, for $\varepsilon_{r2} = 3$, are depicted in Figures 9(a) and 9(c). The shape of the rough surface is well displayed in Figure 9(a), but the buried cube is not shown there. This is due to the fact that at $t = 15\,\text{ns}$, the incident wave just impinges the rough surface but has not reached the buried cube yet. As the time progresses, the wave travels farther and at $t = 30\,\text{ns}$, the buried PEC cube is illuminated and its shape is well represented in Figure 9(c). In order to demonstrate

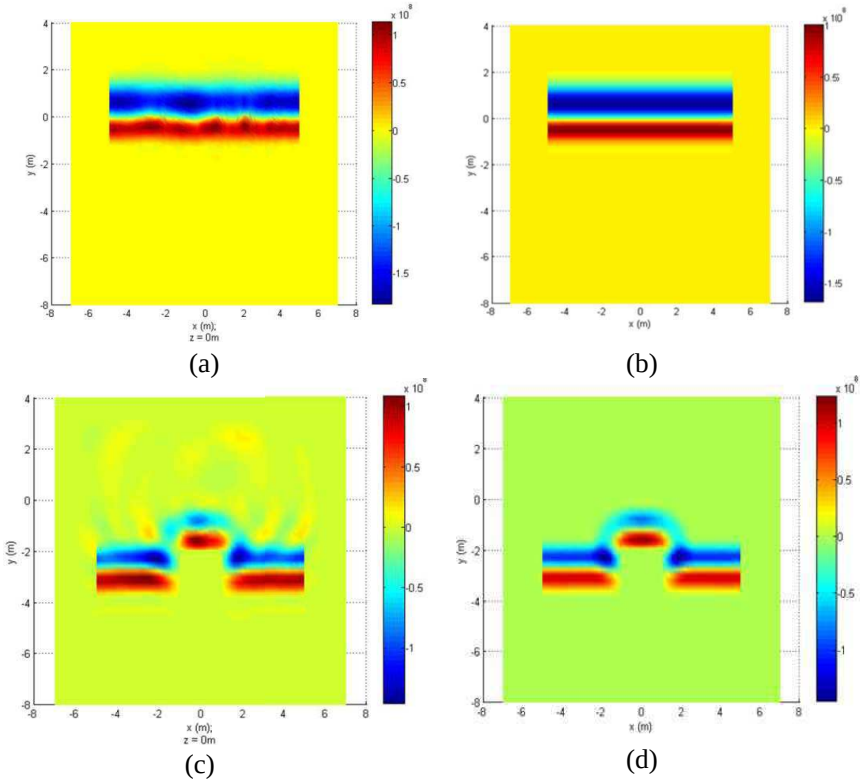

Figure 9. Spatial distribution of the electric field on the $z = 0$ plane, (a) with a random rough interface, observed at $t = 15$ ns; (b) with a flat interface, observed at $t = 15$ ns; (c) with a random rough interface, observed at $t = 30$ ns; (d) with a flat interface, observed at $t = 30$ ns.

the impact of the roughness of the interface on the scattering, the spatial distribution of E_z with a flat media interface at $t = 15$ ns and $t = 30$ ns are illustrated in Figures 9(b) and 9(d). From a comparison between the data shown in Figure 9(a) with 9(b) and Figure 9(c) with Figure 9(d), one observes a significant difference, which is due to the impact of the rough surface.

3.4. Scattering of a Dielectric Cube Buried below a Random Rough Surface

Next, we present the numerical results of scattering of a dielectric cube with side length of 0.6 m and centered at $(0, -0.9, 0)$, buried below a

random rough surface. The random rough surface is of correlation length $l_c = 0.12\,\text{m}$, *rms* height $h_{rms} = 0.1\,\text{m}$, and located within $-1.2 \leq x \leq 1.2$, $-0.9 \leq z \leq 0.9$. The upper half space is free space, and the lower half space is characterized by $\varepsilon_{r2} = 2$. The incident plane wave is with $f_c = 200\,\text{MHz}$. The numerical results of E_z observed at (0, 0.6, 0) are depicted in Figure 10 for the relative permittivity of the dielectric cube ε_{r3} varying from 2 to 3, and then to 4. As shown in this figure, before the moment $t \approx 9\,\text{ns}$, the electric field E_z does not change as ε_{r3} varies because the filed then is due to the scattering of the lower half space only, the relative permittivity of which remains to be unchanged. But after that moment, the scattering from the dielectric cube reaches the observation point and it changes for different ε_{r3}, as it is supposed to be. Note that for $\varepsilon_{r3} = 2$, which is equal to the relative permittivity of the lower half space ε_{r2}, there is no scattering from the dielectric cube and the scattering is from the rough surface only, as illustrated by the dotted green line. But as ε_{r3} is increased to 3 and then to 4, the scattering from the dielectric cube shows up and becomes stronger for larger ε_{r3}, as expected.

3.5. Scattering of a Dielectric Square Cylinder Buried below a Random Rough Surface with Various Roughness

To illustrate the capacity of the Monte-Carlo MPSTD method presented in this paper, in this section, we consider a buried dielectric square cylinder, with a cross sectional area of $0.6\,\text{m} \times 0.6\,\text{m}$ and a length of 1.8 m, buried below a random rough surface with various roughness. The top surface of the buried square cylinder is located 0.6 m below

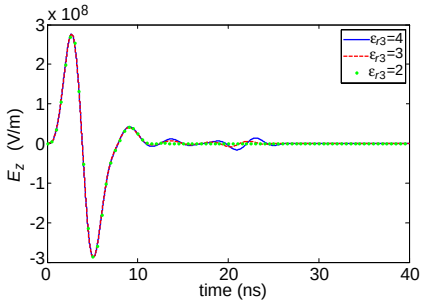

Figure 10. Scattering from a dielectric cube buried below a random rough surface observed at (0, 0.6, 0) for various ε_{r3}.

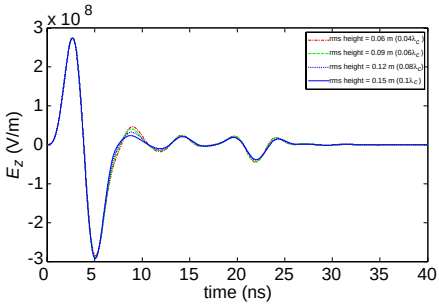

Figure 11. Scattering from a dielectric square cylinder buried below a random rough surface observed at (0, 0.6, 0) for various *rms* height h_{rms}.

$y = 0$ where the rough surface is located. The incident plane wave is with central frequency $f_c = 200\,\text{MHz}$, the lower half space is taken to be of relative permittivity $\varepsilon_{r2} = 2$ and the dielectric square cylinder is characterized by $\varepsilon_{r3} = 4$. The roughness of the random rough surface can be described by its *rms* slope $s = \frac{\sqrt{2}h_{rms}}{l_c}$ [36]. The correlation length of the random rough surface is taken to be $l_c = 0.12\,\text{m}\,(0.08\lambda)$, and its *rms* height h_{rms} varies from $0.06\,\text{m}\,(0.04\lambda)$, to $0.09\,\text{m}\,(0.06\lambda)$, then $0.12\,\text{m}\,(0.08\lambda)$, and finally $0.15\,\text{m}\,(0.1\lambda)$, which correspond to $s = 0.707$, 1.06, 1.4142, and 1.7678, respectively. The numerical results are presented in Figure 11. It has been found from the numerical tests that the solution is stable for $h_{rms} = 0.06\,\text{m}$, $0.09\,\text{m}$, and $0.12\,\text{m}$ using a time step length $\Delta t = 5\,\text{ns}$. But for $h_{rms} = 0.15\,\text{m}$, the solution becomes unstable. However, the solution regains its stability after the time step is decreased to $\Delta t = 2\,\text{ns}$, at a cost of longer computation time. This numerical example demonstrates that the Monte-Carlo MPSTD method presented can solve the scattering problem involving a pretty rough random rough surface with its *rms* slope up to $s = 1.7678$. For comparison, in the literature, for examples, a rough surface with $l_c = 0.2\,\text{m}$ and $h_{rms} = 0.1\,\text{m}\,(s = 0.707)$ is considered in [17]; $l_c = 0.2\lambda$ and $h_{rms} = 0.01\lambda\,(s = 0.0707)$ are used in [4].

Also, the size of the buried object and the distance between the buried object and the rough surface are important parameters that must be considered in the Monte-Carlo MPSTD method. Apparently, the size of the buried dielectric square cylinder, with a cross sectional area of $0.6\,\text{m} \times 0.6\,\text{m}$ and a length of $1.8\,\text{m}$, analyzed in this section is larger than the dielectric cube with side length of $0.6\,\text{m}$ considered in the previous example. Such a larger buried object has been successfully treated by increasing the number of grids of the subdomain occupied by the buried object without adding more subdomains. If the distance between the buried object and the rough surface is larger, then more grids and/or more computation domains would be needed at a cost of more computation time.

3.6. Scattering of a Dielectric Sphere Buried below a Random Rough Surface

The last example is for the scattering of a lossy dielectric sphere buried below a random rough surface. The geometry and the electromagnetic parameters of the sphere and the incident wave are taken to be the same as those used for Figure 5. The random rough surface is of correlation length $l_c = 0.4\,\text{m}$, the *rms* height $h_{rms} = 0.2\,\text{m}$, and it is located by $-4 \le x \le 4$, $-2 \le z \le 2$. The numerical results of E_z observed at (0, 2, 0) and (−1, 2, −2) are presented in Figure 12 for the lower-half-

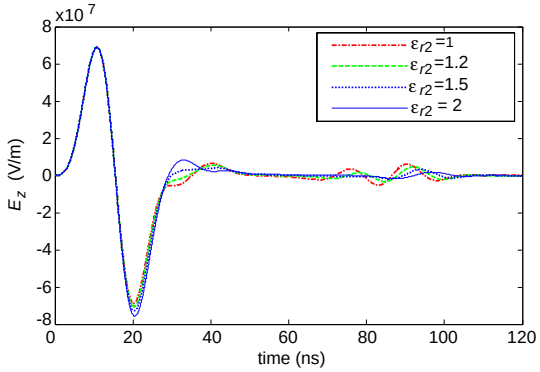

Figure 12. Scattering from a dielectric sphere buried below a random rough surface observed at (0, 2, 0) for various ε_{r2}.

space relative permittivity ε_{r2} varying from 1 to 1.2, then to 1.5, and finally to 2. From this figure, one observes that as $\varepsilon_{r2} = 1$, which is equivalent to the problem of scattering of the dielectric sphere in free space, the result is exactly the same as that shown in Figure 5(b), as expected. And when ε_{r2} is gradually increased from 1 to 2, the effects of the random rough surface appears and it gradually dominates the scattering.

4. CONCLUSIONS

A Monte-Carlo MPSTD algorithm is formulated and implemented for studying the scattering of a 3D object buried below a random rough surface of finite length. The 3D object may be of various shapes and electromagnetic properties; embedded in a half space with different permittivity and the roughness of the random rough surface may vary. Sample numerical results are presented, validated, and analyzed. Through the analysis, it is shown that the roughness of the random rough surface and the electromagnetic properties of the lower half space can significantly affect the scattered signature of the buried object. In addition, the numerical results show that the Monte-Carlo MPSTD method presented in this paper can handle a pretty rough random rough surface involved in the scattering problem, the roughness of which represented by the *rms* slope may be up to $s = 1.7678$. Currently, the authors are extending the Monte-Carlo MPSTD algorithm presented in this paper to the analysis of scattering of an object buried below an infinitely-long random rough surface, and finally extend it for determining the scattering of a 3D object buried in a layered half space with random rough interfaces.

ACKNOWLEDGMENT

The authors appreciate the financial support provided by the National Science Foundation to this work, under award number 0821918. Also, the authors thank Profs. Q. H. Liu and Y. Chen for helpful technical discussions. Special thanks from the authors go to Prof. Y. Shi and Dr. G. X. Fan for their helpful suggestions/comments during numerous detailed technical discussions.

REFERENCES

1. Wang, M.-J., Z.-S. Wu, and Y.-L. Li, "Investigation on the scattering characteristics of Gaussian beam from two dimensional dielectric rough surfaces based on the Kirchhoff approximation," *Progress In Electromagnetic Research B*, Vol. 4, 223–235, 2008.
2. Guo, L.-X., Y. Liang, J. Li, and Z.-S. Wu, "A high order integral SPM for the conducting rough surface scattering with the tapered wave incidence-TE case," *Progress in Electromagnetic Research*, Vol. 114, 333–352, 2011.
3. Berginc, G., "Small-slope approximation method: A further study of vector wave scattering from two-dimensional surfaces and comparison with experimental data," *Progress In Electromagnetics Research*, Vol. 37, 251–287, 2002.
4. Lawrence, D. E. and K. Sarabandi, "Electromagnetic scattering from a dielectric cylinder buried beneath a slightly rough surface," *IEEE Transactions on Antennas and Propagation*, Vol. 50, No. 10, 1368–1376, 2002.
5. Fiaz, M. A., F. Frezza, L. Pajewski, C. Ponti, and G. Schettini, "Scattering by a circular cylinder buried under a slightly rough surface: The cylindrical-wave approach," *IEEE Transactions on Antennas and Propagation*, Vol. 60, No. 6, 2834–2842, 2012.
6. Wang, X. and L.-W. Li, "Numerical characterization of bistatic scattering from PEC cylinder partially embedded in a dielectric rough surface interface: Horizontal polarization," *Progress In Electromagnetics Research*, Vol. 91, 35–51, 2009.
7. Zhang, G. F., L. Tsang, and K. Pak, "Angular correlation function and scattering coefficient of electromagnetic waves scattered by a buried object under a two-dimensional rough surface," *J. Opt. Soc. Am. A*, Vol. 15, No. 12, 2995–3002, 1998.
8. Johnson, J. T., "A numerical study of scattering from an object above a rough surface," *IEEE Transactions on Antennas and Propagation*, Vol. 48, No. 1, 1361–1367, 2002.

9. El-Shenawee, M., C. Rappaport, E. Miller, and M. Silevitch, "3-D subsurface analysis of electromagnetic scattering from penetrable/PEC objects buried under rough surface: Use of the steepest descent fast multipole method (SDFMM)," *IEEE Transactions on Geoscience and Remote Sensing*, Vol. 39, No. 6, 1174–1182, 2001.
10. El-Shenawee, M., "Scattering from multiple objects buried beneath two-dimensional random rough surface using the steepest decent fast multipole method," *IEEE Transactions on Antennas and Propagation*, Vol. 51, No. 4, 802–809, 2003.
11. Ji, W.-J. and C.-M. Tong, "Bistatic scattering from two-dimensional dielectric ocean rough surface with a PEC object partially embedded by using the GSMCG method," *Progress In Electromagnetics Research*, Vol. 105, 119–139, 2010.
12. Chen, H. T. and G.-Q. Zhu, "Model the electromagnetic scattering from three-dimensional PEC object buried under rough ground by MoM and modified PO hybrid method," *Progress In Electromagnetics Research*, Vol. 77, 15–27, 2007.
13. Ye, H. X. and Y. Q. Jin, "A hybrid analytic-numerical algorithm of scattering from an object above a rough surface," *IEEE Transactions on Geoscience and Remote Sensing*, Vol. 45, No. 5, 1174–1180, 2007.
14. Guan, B., J. F. Zhang, X. Y. Zhou, T. J. Cui, and W. Hong, "Electromagnetic scattering from objects above a rough surface using the method of moments with half-space Green's function," *IEEE Transactions on Geoscience and Remote Sensing*, Vol. 47, No. 10, 3309–3405, 2009.
15. Li, X.-M., C.-M. Tong, S. H. Fu, and J.-J. Li, "Bistatic electromagnetic scattering from a three-dimensional perfect electric conducting object above a Gaussian rough surface based on the Kirchhoff-Helmoltz and electric field integral equation," *Waves in Random and Complex Media*, Vol. 21, No. 3, 389–404, 2011.
16. Hastings, F. D., J. B. Schneider, and S. L. Broschat, "A Monte-Carlo FDTD technique for rough surface scattering," *IEEE Transactions on Antennas and Propagation*, Vol. 13, No. 11, 1183–1191, 1995.
17. Kuang, L. and Y.-Q. Jin, "Bistatic scattering from a three-dimensional object over a randomly rough surface using the FDTD algorithm," *IEEE Transactions on Antennas and Propagation*, Vol. 49, No. 11, 2302–2312, 2007.
18. Li, J., L.-X. Guo, and H. Zeng, "FDTD investigation on the

electromagnetic scattering from a target above a randomly rough surface," *Waves in Random and Complex Media*, Vol. 18, No. 4, 641–650, 2008.

19. Dridi, K. H., J. S. Hesthaven, and A. Ditkowski, "Staircase-free finite-difference time-domain formulation for general materials in complex geometries," *IEEE Transactions on Antennas and Propagation*, Vol. 49, No. 5, 749–756, 2001.
20. Hastings, F. D., J. B. Schneider, and S. L. Broschat, "A finite-difference time-domain solution to scattering from a rough pressure-release surface," *Journal of American Acoustic Society*, Vol. 102, No. 6, 3394–3400, 1997.
21. Liu, Q. H., "The PSTD algorithm: A time-domain method requiring only two cells per wavelength," *Microwave and Optical Technology Letters*, Vol. 15, No. 3, 158–165, 1997.
22. Taflove, A. and S. C. Hagness, *Computational Electrodynamics the Finite-difference Time-domain Method,* 3rd Edition, Chapter 17, Advances in PSTD Techniques, Q. H. Liu and G. Zhao, Eds., Artech House, Inc., Norwood, MA, 2005.
23. Yang, B. and J. S. Hesthaven, "A pseudospectral method for time-domain computation of electromagnetic scattering by bodies of revolution," *IEEE Transactions on Antennas and Propagation*, Vol. 47, No. 1, 132–141, 1999.
24. Yang, B. and J. S. Hesthaven, "Multidomain pseudospectral computation of Maxwell's equations in 3-D general curvilinear coordinates," *Applied Numerical Mathematics*, Vol. 33, 281–289, 2000.
25. Zhao, G. and Q. H. Liu, "The 2.5-D multidomain pseudospectral time-domain algorithm," *IEEE Transactions on Antennas and Propagation*, Vol. 51, No. 3, 619–627, 2003
26. Zhao, G. and Q. H. Liu, "The 3-D multidomain pseudospectral time-domain algorithm for inhomogeneous conductive media" *IEEE Transaction on Antennas and Propagation*, Vol. 52, No. 3, 742–749, 2003.
27. Shi, Y. and C.-H. Liang, "Two dimensional multidomain pseudospectral time-domain algorithm based on alternating-direction implicit method," *IEEE Transactions on Antennas and Propagation*, Vol. 54, No. 4, 1207–1214, 2006.
28. Shi, Y. and C.-H. Liang, "Multidomain pseudospectral time domain algorithm using a symplectic integrator," *IEEE Transactions on Antennas and Propagation*, Vol. 55, No. 2, 433–439, 2007.
29. Liu, Q. H., "Large-scale simulations of electromagnetic and

acoustic measurements using the pseudospectral time-domain (PSTD) algorithm," *IEEE Transactions on Geoscience and Remote Sensing*, Vol. 37, No. 2, 917–926, 1999.

30. Liu, Q. H. and G.-X. Fan, "Simulations of GPR in dispersive media using a frequency-dependent PSTD algorithm," *IEEE Transaction on Geoscience and Remote Sensing*, Vol. 37, No. 5, 2317–2324, 1999.
31. Fan, G. X., Q. H. Liu, and J. S. Hesthaven, "Multidomain pseudospectral time-domain simulations of scattering by objects buried in lossy media," *IEEE Transactions on Geoscience and Sensing*, Vol. 40, No. 6, 1366–1373, 2002.
32. Liu, W., Y. Dai, H.-Y. Yang, and X.-B. Xu, "Scattering of object buried below random rough surface — A Monte Carlo pseudospectral time-domain approach," *Electromagnetics*, Vol. 32, No. 6, 330–344, 2012.
33. Fan, G.-X. and Q. H. Liu, "A well-posed PML absorbing boundary condition for lossy media," *Proceedings of IEEE Antennas and Propagation Society International Symposium*, Vol. 3, 2–5, 2001.
34. Fan, G.-X. and Q. H. Liu, "A strongly well-posed PML in lossy media," *IEEE Antennas and Wireless Propagation Letters*, Vol. 2, 97–100, 2003.
35. Shi, Y. and C.-H. Liang, "A strongly well-posed PML with unsplit-field formulations in cylindrical and spherical coordinates," *Journal of Electromagnetic Waves and Applications*, Vol. 19, No. 13, 1761–1776, 2005.
36. Tsang, L., J. A. Kong, K. H. Ding, and C. O. Ao, *Scattering of Electromagnetic Waves, (Volume II) Numerical Simulations*, John Wiley & Sons Inc., New York, 2001.
37. Papoulis, A., *Probability, Random Variables, and Stochastic Processes*, 2nd Edition, McGraw-Hill Book Company, New York, 1984.
38. Sadiku, M. N. O., *Numerical Techniques in Electromagnetics*, CRC Press, 1992.